DOI: 10.1055/s-0039-1677863

POSTPRINT
VERSION

Three-Dimensional Surface Reconstruction of the Human Cochlear Nucleus: Implications for Auditory Brain Stem Implant Design

Osama Tarabichi[1,*] Vivek V. Kanumuri[1,2,*] Julian Klug[1,3] Nicolas Vachicouras[4] Maria J. Duarte[1] Lorenz Epprecht[1] Elliott D. Kozin[1,2] Katherine Reinshagen[5] Stéphanie P. Lacour[4] M Christian Brown[1,2] Daniel J. Lee[1,2]

[1] Department of Otolaryngology – Head and Neck Surgery, Massachusetts Eye and Ear Infirmary, Boston, Massachusetts, United States
[2] Department of Otology and Laryngology, Harvard Medical School, Boston, Massachusetts, United States
[3] Faculty of Medicine, University of Geneva, Switzerland
[4] Bertarelli Foundation Chair in Neuroprosthetic Technology, Laboratory for Soft Bioelectronic Interfaces, Centre for Neuroprostheses, École Polytechnique Fédérale de Lausanne (EPFL), Switzerland
[5] Department of Radiology, Massachusetts Eye and Ear Infirmary, Boston, Massachusetts, United States

Address for correspondence Daniel J. Lee, MD, FACS, Massachusetts Eye and Ear Infirmary, Harvard Medical School, 243 Charles Street, Boston, MA 02114, United States (e-mail: Daniel_Lee@meei.harvard.edu).

Abstract

Objective The auditory brain stem implant (ABI) is a neuroprosthesis placed on the surface of the cochlear nucleus (CN) to provide hearing sensations in children and adults who are not candidates for cochlear implantation. Contemporary ABI arrays are stiff and do not conform to the curved brain stem surface. Recent advancements in microfabrication techniques have enabled the development of flexible surface arrays, but these have only been applied in animal models. Herein, we measure the surface curvature of the human CN and adjoining regions to assist in the design and placement of next-generation conformable clinical ABI arrays. Three-dimensional (3D) reconstructions from ultrahigh T1-weighted brain magnetic resonance imaging (MRI) sequences and histologic reconstructions based on postmortem adult human brain stem specimens were used.

Design This is a retrospective review of radiologic data and postmortem histologic axial sections.

Setting This is set at the tertiary referral center.

Participants Data were acquired from healthy adults.

Main Outcome Measures The main outcome measures are principal curvature values (Kmin and Kmax) and global radius of curvature.

Results The CN was successfully extracted and rendered as a 3D surface in all cases. Significant curvatures of the CN in both histologic and radiographic reconstructions

Keywords

- auditory brain stem implant
- cochlear nucleus
- curvature
- surface curvature

* *These authors contributed equally to this study.*

Dr. Lorenz Epprecht's ORCID is http://orcid.org/0000-0002-1295-8908.
Dr. Osama Tarabichi's ORCID is http://orcid.org/0000-0002-0877-4698.

received
June 4, 2018
accepted after revision
December 15, 2018

were found with global radius of curvature ranging from 2.08 to 8.5 mm. In addition, local curvature analysis revealed that the surface is highly complex.

Conclusion Detailed rendering of the human CN is feasible using histology and 3D MRI reconstruction and highlights complex surface topography that is not recapitulated by contemporary stiff ABI arrays.

Introduction

The auditory brain stem implant (ABI) provides sound awareness for adults and children with neurofibromatosis type 2 (NF2) or other conditions associated with cochlea or cochlear nerve pathology.[1–4] ABI surgery necessitates a craniotomy approach and blind placement of a rigid surface multichannel array via the lateral recess of the fourth ventricle on or near the surface of the cochlear nucleus (CN).[5] Appropriate placement is verified electrophysiologically using intraoperative responses evoked by electrical stimulation with the surface array (electrically evoked auditory brain stem responses). Overall, the ABI enables patients to achieve gains in auditory perception; however, these patients perform significantly worse than those with cochlear implants in several outcome measures such as speech comprehension.[6,7] In addition, ABI users often experience side effects due to stimulation of nonauditory axons of passage that in some cases renders the implant unusable.[8–11]

The reasons for modest auditory outcomes among ABI users compared with cochlear implant (CI) users are several intractable and tractable factors. Intractable factors include damage to the CN caused by a tumor and/or its removal[12,13] and nonoptimal placement of the ABI electrode array[14] due to blind placement and a small neural target.[13] A potentially tractable cause of poor performance is that current generation ABI arrays are stiff and do not conform to the curved surface of the brain stem. This can result in poor electrode contact with the brain stem surface, increasing electrode impedance and off-target effects from current spread, and reducing spectral resolution.

Recent advancements in flexible electronics and materials science have allowed for the development of electrode arrays that can be built on a flexible substrate. The functionality, durability, and biocompatibility of these arrays have been tested in primate and rodent models of the ABI and of spinal cord injury.[15,16] In a spinal cord rodent model, flexible arrays were associated with reduced inflammation and deformation of the neural interface compared with rigid designs.[16] Polymers used in these substrates can be engineered to match the elastic properties of neural tissue and their flexibility can be tuned to better approximate the curved brain or spinal cord surface.[15,17,18] The ability of these arrays to conform to a surface is due to a physical phenomenon termed "capillarity-induced folding."[19] This phenomenon dictates that the elasticity and thickness of the material or sheet (in this study—ABI array) determine how curved of a surface the array can conform to. Therefore, a basic understanding of the degree of curvature of the target region is invaluable in designing a conformable array. To date, no study has been performed that specifically examines the surface curvature of the human CN (the target of the ABI). Herein, we describe a novel approach for three-dimensional (3D) reconstruction and a topographic analysis of the CN using human histologic specimens. To assess the feasibility of performing these measurements radiographically, we then reproduced our topographic analysis on CN reconstructions obtained from a single ultrahigh-resolution magnetic resonance imaging (MRI) dataset enabled by sophisticated motion detection methods.

Materials and Methods

Data Acquisition

This study was approved by our Human Studies Committee (#1447618, exempt). Postmortem human brain stem sections of the left CN from three healthy adult patients were used for histological reconstruction. Axial brain stem sections 10 to 20 m in thickness were alternatively stained with protargol, cresyl violet Nissl stain, or hematoxylin.

Ultrahigh-resolution MRI sequences were obtained from Lusebrink et al.[20,21] Imaging data were acquired from a healthy 34 years old using a 7-Tesla MRI. Ultrahigh resolution was obtained using accurate motion correction techniques that can detect microscopic motion. The resulting voxels with isotropic resolution of 250 µm are 64 times smaller than the standard clinical resolution of 1 mm and required 8 hours of scan time to achieve.

3D Surface Reconstructions

For histologic specimens, the CN was identified using light microscopy and its borders were manually traced in each relevant section. Laterality selection (left vs. right) was based on overall ease of CN identification and quality of preservation in sections. Sections were aligned using vessels, histologic artifacts, and other features that remained consistent between sections. Images of tracings were then imported into segmentation software (Amira; TGS, Berlin, Germany) for 3D reconstruction and rendering of specific regions of interests. A surface mesh was then created and exported as a MATLAB (Mathworks, Massachusetts, United States) file for further curvature analysis (►**Fig. 1**).

For radiographic analysis, a single ultrahigh-resolution T1-weighted MRI series (250 microns isotropic voxel resolution) was imported to Amira. Regions of interest were selected on axial, coronal, and sagittal views to include the CN along with neighboring brain stem structures. 3D surface rendering of selected regions was then performed (►**Fig. 1**).

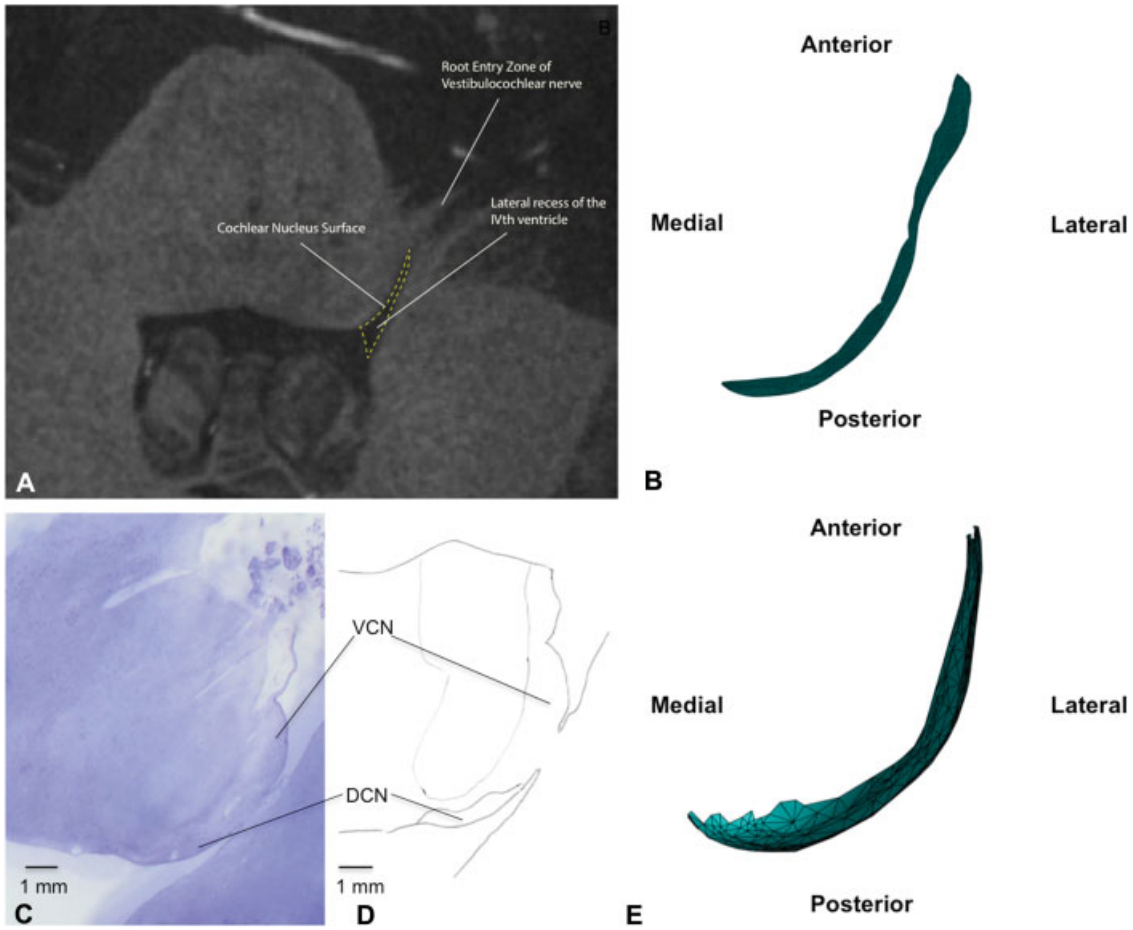

Fig. 1 CN surface extraction from high-resolution MR data and postmortem axial histological sections. (A) Axial slice of CN from ultrahigh T1-weighted scan. (B) Extracted CN surface. The surface invariably included other structures that reside close to the CN on the posterolateral surface of the brain stem as the borders of CN are not well defined on MRI. (C, D) Axial histological section of CN and corresponding manual trace. (E) Extracted CN surface reconstruction from traces of histological sections. CN, cochlear nucleus; MRI, magnetic resonance imaging.

The 3D surface reconstruction was then exported as a MATLAB file for curvature analysis. Determination of anatomical location of the CN was made by examining surrounding relevant structures such as the inferior cerebellar peduncles (ICPs), cerebellopontine angle, and auditory nerve. In summary, the steps performed to arrive at our final extracted surface were: (1) surface rendering of entire brain/skull extracted from MRI, (2) skull deletion, (3) region of interest selection to include the surface of the CN, (4) selection of approximate location of the CN based on surrounding anatomical structures, and (5) extraction of the surface of the CN and exportation as a MATLAB file.

Local Curvature Computation

Curvature of a surface at any given point in 3D Euclidean space can be computed mathematically (i.e., the local curvature). Given any point P on surface S, curvature is defined in several different two-dimensional (2D) planes normal to the tangent of the curved surface at P as the inverse of the radius of the osculating circle. The principal curvatures, Kmin and Kmax, are defined as the smallest and largest curvature values obtained from all the different possible curvature values at that given point P. Kmin and Kmax can be used to determine the approximate shape of a surface at a given point.[22] Algorithms were custom written in MATLAB to read the exported surfaces and measure Kmin and Kmax at every point defined to be part of the exported surface, based on published mathematical analyses of curvature.[23,24] After determining the Kmin and Kmax at each point, Kmin–Kmax scatter plots and heat maps were generated to estimate the distribution of curvature and complexities of each surface.

Global Curvature Computation

We also quantified the overall curvature for the entire surface (rather than for each individual point on the surface as in the earlier methodology). The surface of both histologic and radiologic reconstructions were exported as 3D point clouds (based on the vertices of the surface mesh) and were fit to a sphere in a least square sense using a custom MATLAB algorithm.[25] The radius of this best fit sphere was then referred to as "global radius of curvature" and compared between patients. A larger radius of curvature reflects a more "flat" surface, while a smaller radius of curvature reflects a more curved surface.

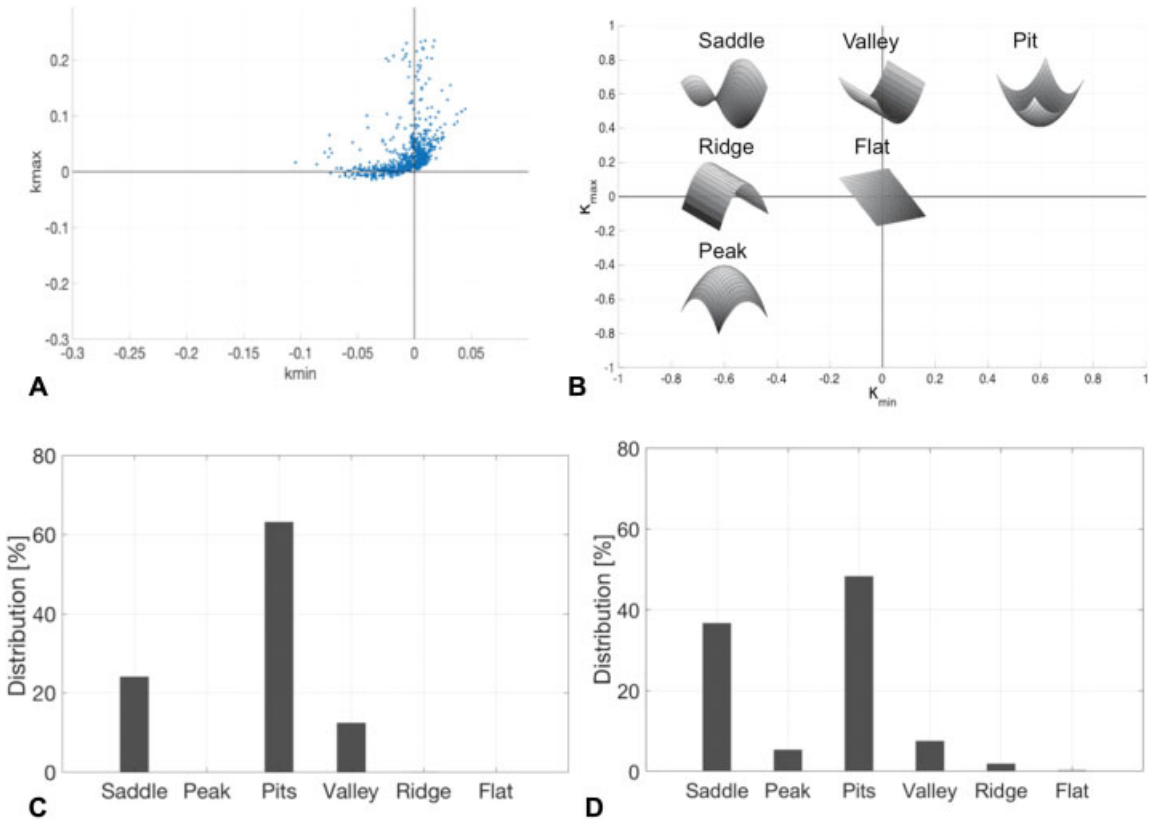

Fig. 2 Local curvature analysis by principal curvature computation. (A) Kmin–Kmax scatter plots of representative reconstructed CN surface extracted from histologic specimens. (B) Graphical representation of classification of shapes relative to Kmin–Kmax plot. Kmin and Kmax are the principal curvatures observed at each point along the surface of the exported CN. Spatial distribution of Kmin–Kmax data points on to the above figure can be used to approximate what shape each of our rendered surfaces most closely resembles. Shapes based on descriptions from Besl et al and Besl et al.[22] (C) Bar plot of average distribution of shape observed at each point in the radiographic CN reconstruction. Surface is predominantly pit and saddle-shaped. (D) Bar plot of distribution of shape observed at each point across all three histologic reconstructions of cochlear nuclear surfaces. Surface is predominantly saddle and pit-shaped. CN, cochlear nucleus.

Results

3D Surface Rendering of the Cochlear Nucleus

Histological and radiologic data were successfully extracted and rendered as a 3D surface from four subjects. One left-sided CN was reconstructed from ultrahigh-resolution radiographic data. Three left-sided CNs were reconstructed from postmortem histologic data.

Computation of Surface Curvature Demonstrates Highly Complex Brain Stem Topography

Surface curvature measurements were made from 3D surface reconstructions of the CN (►**Fig. 1**). Local curvature (►**Figs. 2** and **3**) scatter plots and heat maps of the exported surfaces demonstrate that the surface of the CN is not only curved but also highly complex and irregular. Wide inter-subject variability is noted in principal curvature values with ranges of: Kmin (−1.40 to 0.12) and Kmax (−0.04 to 1.12) for histologic specimens and Kmin (−0.17 to 0.03) and Kmax (−0.06 to 0.13) for the radiographic data. Heat maps provide a visual representation of curvature complexity and revealed high variability of surface curvature in a single CN (►**Fig. 3**).

Most Areas of the Cochlear Nucleus Are Classified as a Nondevelopable Surface

The Kmin and Kmax measures of local curvature can be used to determine the approximate shape of a surface at a given point (►**Fig. 2**). A majority of the points on the CN surface most closely resembled a saddle-shape or a pit in both the histologic and radiologic reconstructions (►**Fig. 2**). Saddles

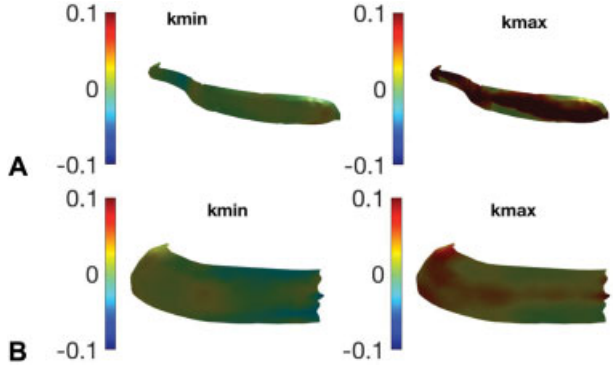

Fig. 3 Kmin and Kmax color maps of reconstructed radiological (A) and histological (B) CN surfaces reveal a complex topography. CN, cochlear nucleus.

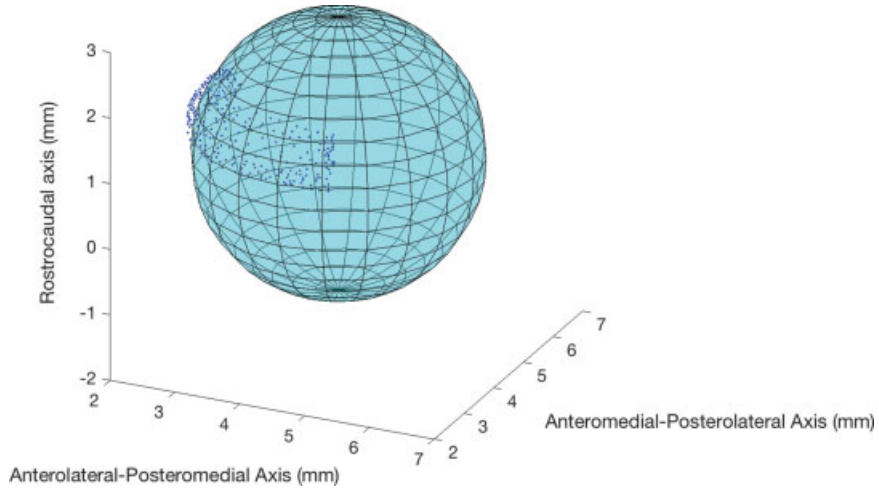

Fig. 4 Global curvature analysis by sphere fitting. CN surface reconstructed from postmortem histological slices with a sphere of best fit plotted against the surface. Radius of the sphere of best fit provides an estimate of the overall curvature of the surface in all Euclidean planes. CN, cochlear nucleus.

and pits are geometrically classified as nondevelopable surfaces, meaning that they cannot be constructed by transforming a 2D plane (such as a flat, rigid array).

Global Curvature Analyses Reveal a Curved Surface Overall

Global curvature measures such as the radius of curvature obtained by the sphere-fit algorithm also suggest that in both histologic and radiographic reconstructions, the CN is highly curved (►**Fig. 4**). The global radius of curvature ranged from 2.08 to 4.52 mm (mean 3.15 ± 1.24) in histologic specimens and 8.5 mm in the radiographic specimen.

Discussion

Our study is the first to systematically examine the curved surface of the human auditory brain stem and specifically the CN (the target of the ABI) and surrounding anatomy. Using histologic specimens and publicly available ultrahigh-resolution MRI sequence, we were able to perform 3D reconstruction of our regions of interest. We used both histologic and radiographic data as each dataset carries distinct advantages and disadvantages. For example, in histologic reconstructions, the borders of the dorsal CN can be precisely identified using stains that highlight neuronal cell bodies and myelin (e.g., Nissl). However, postmortem preparation introduces desiccation and fixation artifacts that may flatten the surface when compared with in vivo brain stem tissue.

The structural T1-weighted imaging that was primarily used for reconstruction in our study had an ultrahigh resolution (250 µm isotropic) compared with standard clinical scans (1 mm isotropic). These imaging data were necessary as it is virtually impossible to radiographically resolve the CN surface from adjacent ICP using standard clinical imaging. This fourfold decrease in isotropic resolution yields voxels that are 64 times smaller and allow us to resolve the CN from the ICP and the lateral recess of the fourth ventricle and select a region that almost certainly contains the CN surface. This level of resolution was achieved by Lusebrink et al using sensitive motion detection methods over a very long scan time (8 hours). The resolution needed to adequately visualize the CN severely limits our sample size but suggests that with more widespread availability of the MRI technology developed by Lüsebrink et al, it would be feasible to obtain in vivo measures of CN curvature.[20] It is important to note however that the gray–white matter contrast on MRI is not sufficient to resolve the CN from surrounding brain stem nuclei and it is therefore difficult to resolve the precise limits of the CN. Identification of the approximate location of the CN surface was aided by the visualization of the path of the eighth cranial nerve as it entered the brain stem and the ability to discriminate among the ICP, lateral recess of the fourth ventricle, and brain stem surface (►**Fig. 1A**).[26,27]

In an attempt to quantify the surface curvature of the resulting reconstructions, we performed a Kmin–Kmax analysis that mathematically classifies each point along the surface. This revealed wide variability in curvature among patients and within each patient's reconstructed brain stem. Global curvature measures using the sphere-fit algorithm similarly varied. This is in line with previous work in anatomic studies that suggest that CN size varies widely among individuals by up to a factor of 3.[26] Similar to our findings, these studies also revealed a spatially complex CN with a distorted silhouette. The shape of the curvature at each point on the CN surface in our study most closely resembled a saddle or pit shape, both nondevelopable surfaces. This is an important parameter that can inform ABI array design as materials must be both *flexible* and *stretchable* to fully conform to a nondevelopable surface.[28] Materials such as polydimethylsiloxane that have been studied in animal models of the ABI and spinal cord have both stretchable and flexible properties and can theoretically achieve full conformability to the complex surface of the CN.[15,16] Measures of global curvature also provide important information that will influence device design. As discussed in the introduction, the thickness of an array influences how curved of a surface it

can conform to.[19] Measuring radius of curvature can inform manufacturers how thin a device has to be to conform to a surface.

Although our radiographic dataset is limited, there are a few notable differences between histologic and radiographic reconstructions. Overall, histologic reconstructions tended to be more curved than the radiologic reconstructions (though this did not reach significance). This may be secondary to the wider area of the brain stem selected in radiographic reconstructions (due to the imprecision of CN localization relative to histology) which may give the appearance of increased "flatness." These differences were also well within range of variance seen in other features of CN anatomy.[26] In addition, histologic reconstructions tended to have wider variation in local curvature measures. This may be due to the much higher resolution of the histologic specimens that also resulted in many more points on each surface reconstruction.

Limitations

The authors acknowledge that despite the advantages described earlier, the exact region of the CN and landmarks (e.g., choroid plexus with its tenia, root entry zone of CN VIII) remains challenging to identify on MRI sequences and the cerebellum/ICP can obscure parts of the dorsal CN. In addition, gradient nonlinearity corrections performed in the context of the structural scans/histology and edge smoothing performed with surface rendering may affect some measures of curvature. Finally, given the small size of CN even when compared with our relatively high-resolution scans, the surface curvature can be subject to image noise/pixelation. In vivo radiological reconstructions and histologic specimens are also likely to vary simply based on the fact that brain stem is constantly subject to cerebrospinal fluid pressure that may cause transient distortions. Histologic specimens also will undoubtedly suffer some degree of shrinkage and fragmentation secondary to fixation and slice preparation. The data we used were also acquired from healthy participants, while the majority of ABI candidates have NF2 who may have a distorted brain stem anatomy. Regardless, we feel that our methodology remains valuable and more widespread availability of ultrahigh-resolution MRI will allow us to analyze larger datasets that include NF2 patients. A flexible ABI would likely cover or at least impinge on both the CN and adjacent structures when conforming to its target. Thus, any measure of the nature of curvature of this approximate region would prove invaluable from an engineering perspective to determine just how flexible a "flexible ABI" would need to be.

Conclusion

Contemporary ABI electrodes are rigid and do not conform to the curved surface of the brain stem. In this study, we created a topographic map of the CN using high-resolution MRI and human histology data to inform future ABI designs. Our findings reveal a complex curvature with wide internucleus and interpatient variability.

Conflict of Interest
None delcared.

References

1 Puram SV, Lee DJ. Pediatric auditory brainstem implant surgery. Otolaryngol Clin North Am 2015;48(06):1117–1148
2 Kaplan AB, Kozin ED, Puram SV, et al. Auditory brainstem implant candidacy in the United States in children 0-17 years old. Int J Pediatr Otorhinolaryngol 2015;79(03):310–315
3 Colletti L, Shannon R, Colletti V. Auditory brainstem implants for neurofibromatosis type 2. Curr Opin Otolaryngol Head Neck Surg 2012;20(05):353–357
4 Colletti V, Shannon RV, Carner M, Veronese S, Colletti L. Progress in restoration of hearing with the auditory brainstem implant. Prog Brain Res 2009;175:333–345
5 Colletti V, Sacchetto L, Giarbini N, Fiorino F, Carner M. Retrosigmoid approach for auditory brainstem implant. J Laryngol Otol Suppl 2000;(27):37–40
6 Nakatomi H, Miyawaki S, Kin T, Saito N. Hearing restoration with auditory brainstem implant. Neurol Med Chir (Tokyo) 2016;56 (10):597–604
7 Puram SV, Barber SR, Kozin ED, et al. Outcomes following pediatric auditory brainstem implant surgery: early experiences in a North American center. Otolaryngol Head Neck Surg 2016;155 (01):133–138
8 Noij KS, Kozin ED, Sethi R, et al. Systematic review of nontumor pediatric auditory brainstem implant outcomes. Otolaryngol Head Neck Surg 2015;153(05):739–750
9 McSorley A, Freeman SR, Ramsden RT, et al. Subjective outcomes of auditory brainstem implantation. Otol Neurotol 2015;36(05): 873–878
10 Behr R, Colletti V, Matthies C, et al. New outcomes with auditory brainstem implants in NF2 patients. Otol Neurotol 2014;35(10): 1844–1851
11 Sanna M, Di Lella F, Guida M, Merkus P. Auditory brainstem implants in NF2 patients: results and review of the literature. Otol Neurotol 2012;33(02):154–164
12 Colletti V, Shannon RV. Open set speech perception with auditory brainstem implant? Laryngoscope 2005;115(11):1974–1978
13 Rosahl SK, Rosahl S. No easy target: anatomic constraints of electrodes interfacing the human cochlear nucleus. Neurosurgery 2013;72(1, Suppl Operative):58–64, discussion 65
14 Barber SR, Kozin ED, Remenschneider AK, et al. Auditory brainstem implant array position varies widely among adult and pediatric patients and is associated with perception. Ear Hear 2017;38(06):e343–e351
15 Guex AA, Vachicouras N, Hight AE, Brown MC, Lee DJ, Lacour SP. Conducting polymer electrodes for auditory brainstem implants. J Mater Chem B Mater Biol Med 2015;3(25):5021–5027
16 Minev IR, Musienko P, Hirsch A, et al. Biomaterials. Electronic dura mater for long-term multimodal neural interfaces. Science 2015; 347(6218):159–163
17 Bloch J, Lacour SP, Courtine G. Electronic dura mater meddling in the central nervous system. JAMA Neurol 2017;74(04):470–475
18 Hirsch A, Michaud HO, Gerratt AP, de Mulatier S, Lacour SP. Intrinsically stretchable biphasic (solid-liquid) thin metal films. Adv Mater 2016;28(22):4507–4512
19 Py C, Reverdy P, Doppler L, Bico J, Roman B, Baroud CN. Capillarity induced folding of elastic sheets. Eur Phys J Spec Top 2009;166 (01):67–71
20 Lüsebrink F, Sciarra A, Mattern H, Yakupov R, Speck O. T_1-weighted in vivo human whole brain MRI dataset with an ultrahigh isotropic resolution of 250 μm. Sci Data 2017;4:170032
21 Lusebrink F, Sciarra A, Mattern H, Yakupov R, Speck O. T1-weighted in vivo human whole brain MRI dataset with an ultrahigh isotropic

resolution of 250 mum. Dryad Digital Repository Web site. Available at: https://datadryad.org/resource/doi:10.5061/dryad.38s74. Updated 2017

22 Besl PJ, Jain RC. Invariant surface characteristics for 3D object recognition in range images. Comput Vis Graph Image Process 1986;33(01):33–80

23 Parra-Denis E, Moulin N, Jeulin D. Three dimensional complex shapes analysis from 3d local curvature measurements. application to intermetallic particles in aluminium alloy 5xxx. Image Anal Stereol 2011;26(03):157–164

24 Cohen-Steiner D, Morvan J. Restricted Delaunay triangulations and normal cycle. J Assoc Comput Mach 2003;•••:312–321

25 Sumith Y. Fast geometric fit algorithm for sphere using exact solution. arXiv.org Web site. Available at:https://arxiv.org/abs/1506.02776. Accessed February 2, 2018

26 Rosahl SK, Rosahl S. Anatomy of the human cochlear nucleus in relation to auditory brainstem implants. World Congress on Medical Physics and Biomedical Engineering. 2009:40–43

27 Quester R, Schröder R. Topographic anatomy of the cochlear nuclear region at the floor of the fourth ventricle in humans. J Neurosurg 1999;91(03):466–476

28 Jeong JW, Shin G, Park SI, Yu KJ, Xu L, Rogers JA. Soft materials in neuroengineering for hard problems in neuroscience. Neuron 2015;86(01):175–186